Crack patterns in desiccating clay–polymer mixtures with varying composition

2010 J. Phys.: Condens. Matter 22 015402

(http://iopscience.iop.org/0953-8984/22/1/015402)

J. Phys.: Condens. Matter **22** (2010) 015402 (8pp) doi:10.1088/0953-8984/22/1/015402

Crack patterns in desiccating clay–polymer mixtures with varying composition

Soma Nag[1], Suparna Sinha[1], Supti Sadhukhan[2], Tapati Dutta[3] and Sujata Tarafdar[1]

[1] Condensed Matter Physics Research Center, Physics Department, Jadavpur University, Kolkata 700032, India
[2] Physics Department, Jogesh Chandra Chaudhuri College, Kolkata 700033, India
[3] Physics Department, St Xavier's College, Kolkata 700016, India

Received 21 July 2009, in final form 21 October 2009
Published 3 December 2009
Online at stacks.iop.org/JPhysCM/22/015402

Abstract
Crack patterns in desiccating clay suspensions are drastically altered by the addition of polymers. In this paper we report a systematic study of the effect of varying the composition of a clay–polymer composite on the formation of crack patterns. Experiments as well as computer simulations have been done. Details of the morphology and fractal dimension of the experimental patterns are observed and the simulation is done on a two-dimensional spring network model. We find a transition from a completely fragmented fractal pattern at high clay content to a continuous film at about 50% clay content. The results of the simulation are in good qualitative agreement with the experiments. The study is expected to be of importance for clay–polymer composites. These can be designed to give improved mechanical and electrical properties for practical applications.

(Some figures in this article are in colour only in the electronic version)

1. Introduction

When a suspension of laponite in methanol is left to dry in a Petri dish, it breaks up into fragments separated by a fractal network of hierarchical cracks [1]. On the other hand, when polyethylene oxide is similarly treated, it forms a continuous uniform film, which has a ductile and plastic nature [2]. It deforms without breaking when subjected to a moderate tensile stress. This observation leads us to expect interesting results when the clay and polymer are mixed together in different proportions and allowed to desiccate. Polymer–clay composites are becoming an important class of materials for practical applications, since they allow tailoring of different physical properties [3, 4]. The objective of this work is to study the formation of desiccation cracks in clay–polymer mixtures through experiments and computer simulations.

2. Experiments

We use the synthetic clay laponite (RD) from Rockwood as the clay component. The polymer is poly(ethylene oxide), PEO (BDH, UK), of molecular weight 6×10^5. 2 g of solute consisting of a fraction Pr of laponite and $1 - Pr$ of PEO is mixed with 50 ml of methanol. It is stirred at room temperature for 30 min in a magnetic stirrer. The suspension is poured into a polypropylene Petri dish of 9.5 cm diameter and allowed to dry. The samples are photographed and the images analyzed using Image Pro Plus software during drying. Sometimes a pinch of dye is added for clarity. The samples are about 0.2–0.5 mm thick, but in the present study we do not concentrate on the effect of varying sample thickness.

2.1. Crack morphology

Figure 1 shows the appearance of the samples for different Pr values after desiccation. For clay fractions around 0.5 and lower, a continuous film is formed, which can be removed from the Petri dish. The film is about 250 μm thick. As seen in the photograph, the film may have many cracks, depending on the composition, but these cracks are not interconnected, so the film does not break up into disjoint pieces. The pure clay forms a very characteristic hierarchical fractal pattern, which

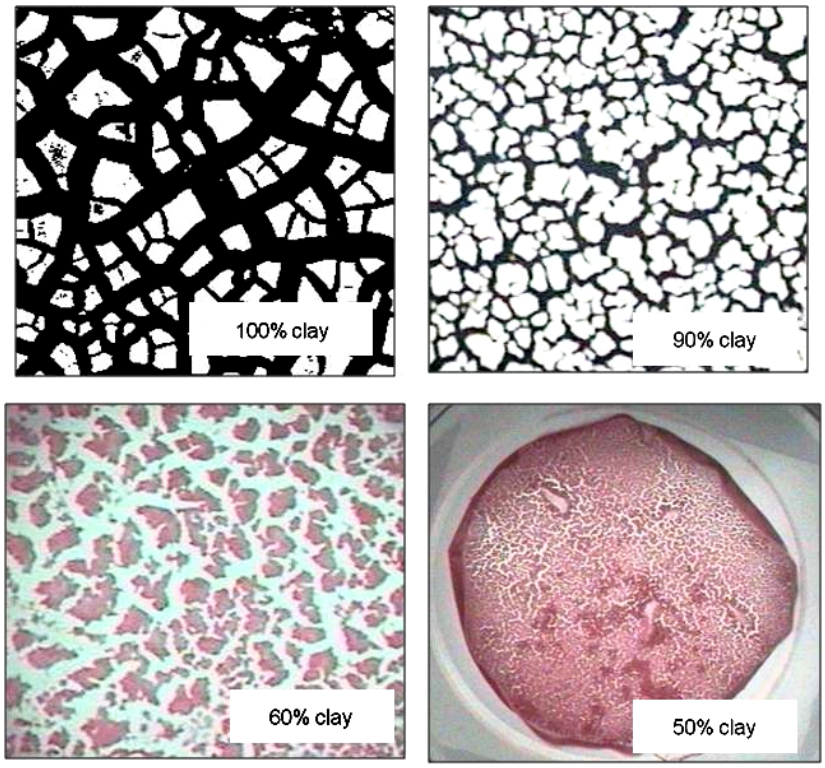

Figure 1. This figure shows crack patterns formed in dried suspensions of clay (laponite) with different fractions of PEO added. In the upper two figures the cracks appear dark and in the lower two the cracks are shown in white. For the 50% clay sample, a continuous film which detaches from the substrate has formed. Many cracks are visible in the continuous film, but they are not interconnected. The side of the three square patterns shown is 6.5 cm.

is well studied and documented [5–8]. In this case cracks are interconnected, forming a network. The cracks have a broad distribution of widths, which separate the solid pieces termed 'peds'. As the polymer is added, the straight outlines of the peds start to get jagged and the broad size distribution of large peds (figure 2) changes drastically (figure 3) as shown in the histograms. The average area of the peds is 400 pixels for pure clay, it falls to 226 for $Pr = 0.9$ and is only 90 for $Pr = 0.8$.

2.2. Crack area

We photographed the crack patterns at certain time intervals during drying. This was done for different compositions. The photographs are grayscaled and the area covered by cracks is measured. Figure 4 shows the area covered by cracks as a function of time for several different clay fractions. For clay fractions 100% and 90% the area increases linearly with time. For lower clay fractions the area increases non-linearly with time and the final crack area is higher than for samples containing more clay. For clay percentages near 50% a continuous film forms, which can be removed from the substrate. We do not measure the crack area for clay content lower than 50%.

2.3. Fractal dimension

A feature of the pattern morphology which is very apparent from figure 1 is the change in the appearance of the ped outline.

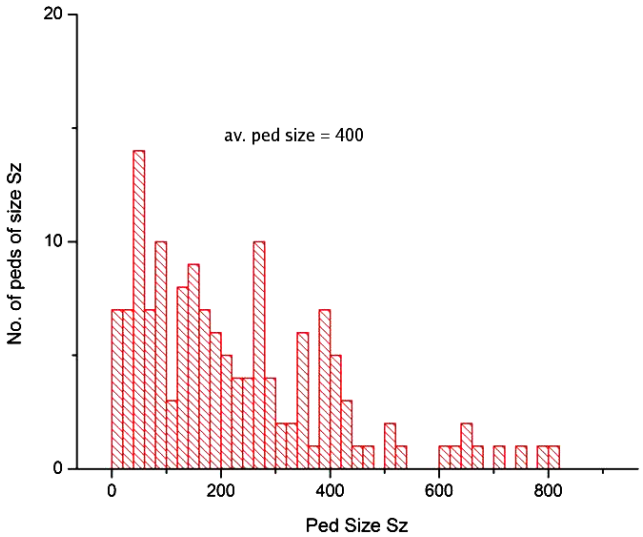

Figure 2. Histogram showing the size distribution of the peds for the pure clay sample. The average area of the peds is 400 pixels. The number of peds of size Sz in pixels is plotted against Sz.

For pure clay ($Pr = 1$), the ped edges look smooth and nearly straight. As soon as a small amount of polymer ($Pr = 0.9$) is introduced, the edges become jagged. The most appropriate way to quantify this feature is through the fractal dimension of the interface. Rather than calculating the fractal dimension

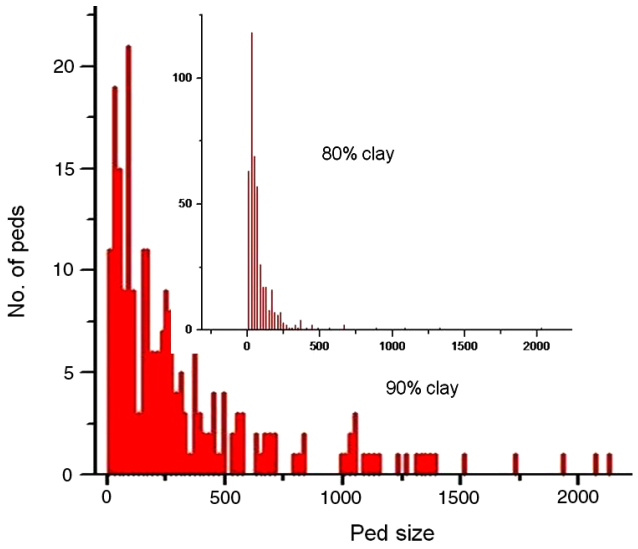

Figure 3. Histograms for the ped size distribution for 90% and 80% clay (inset) samples. For 80% and lower clay fractions, the distribution narrows down to a very large number of peds of very small size, until 50% is reached. Below 50% a continuous film forms.

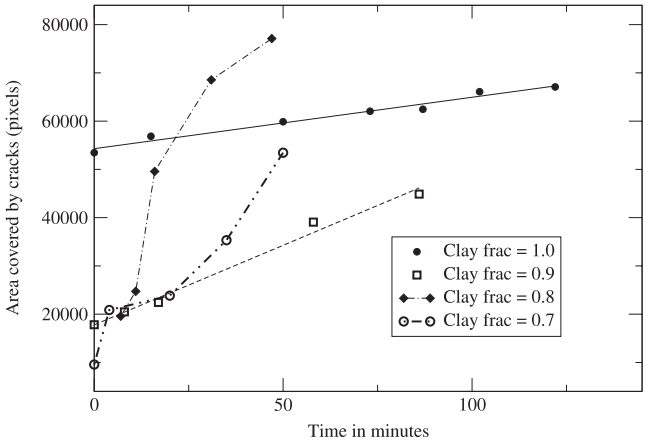

Figure 4. The area covered by cracks as a function of time for different clay–polymer compositions. The final crack area shows an initial decrease at $Pr = 0.9$, but then increases significantly before the continuous film appears. The nature of the time variation also changes from linear to non-linear. However, as this is a highly stochastic process, many more such observations are required to get a true picture.

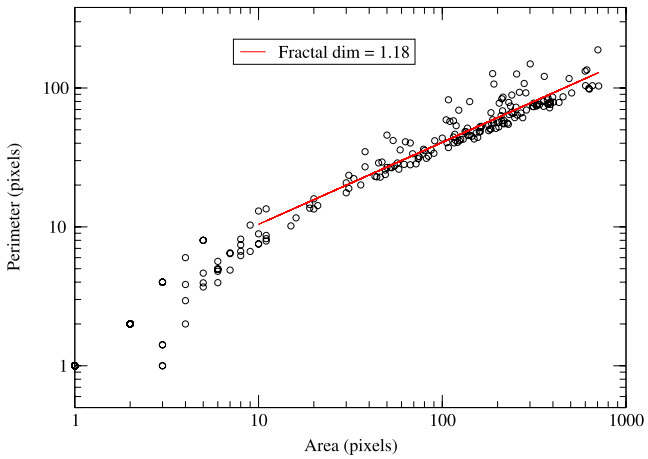

Figure 5. Area–perimeter scaling for peds of a pure clay sample. The line is a power law fit, which gives a $d_f = 1.18$. The smallest peds which do not show the scaling have been omitted from the fit.

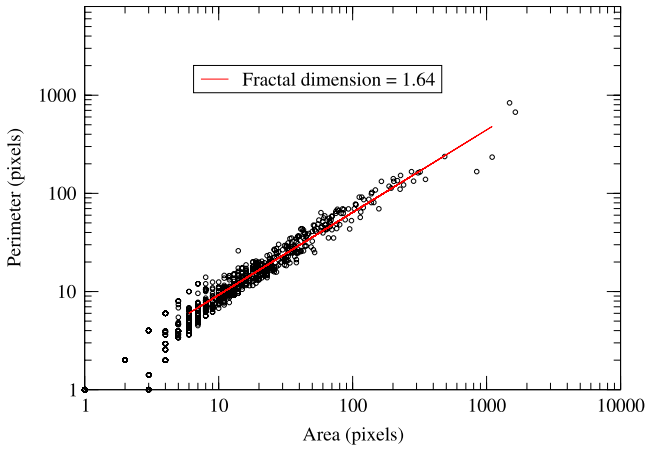

Figure 6. Area–perimeter scaling for peds of a $Pr = 0.5$ sample. The line is a power law fit, which gives $d_f = 1.64$. The smallest peds which do not show the scaling have been omitted from the fit.

of each ped individually, we determine the fractal dimension from the area–perimeter scaling of the whole pattern, which is easily done using Image Pro plus. The log–log scatter plot of the perimeter of each object (here a ped) against its area can be fitted with a straight line, of slope $d_f/2$, where d_f is the interface fractal dimension. This procedure is well known [9, 10] and gives the average d_f for the whole pattern. A perfectly smooth interface should have $d_f = 1$, whereas for self-similar wiggly interfaces, $1 < d_f < 2$.

Figures 5 and 6 show the area–perimeter plots for $Pr = 1.0$ and $Pr = 0.5$, respectively. Values of d_f from the graphs are obtained as 1.14 and 1.64 respectively, clearly illustrating the effect of disorder as polymer is introduced into the clay. Values of d_f for other samples show the same trend. The fractal dimension for pure clay samples lies between 1 and 1.2, while it goes up to about 1.8 with addition of the polymer. This calculation has been done for samples where there is no continuous film, i.e. for $Pr \geqslant 0.5$.

3. The simulation algorithm

In simulating the crack formation in the polymer–clay system, we utilize our code for a two-dimensional spring network, which was developed in [11]. It is modified suitably for the present problem. The top view of the clay–polymer system is represented by a square lattice, with the nodes representing either clay or polymer particles. A fraction Pr of the nodes are randomly assigned to be clay (C); the remainder are polymer (P). Bonds between the nodes are assumed to be springs, which are Hookean up to a certain threshold strain, beyond which they break. We have therefore three kinds of springs, those joining

P–P, C–C and P–C nodes. Each type of spring is characterized by two parameters, a spring constant and a breaking threshold, so there are six spring parameters in all.

Unbalanced forces start to act on the nodes as the system begins to desiccate. A molecular dynamics (MD) approach has been used to calculate the evolution of the system. Desiccation is implemented through a reduction in the natural length of the springs, introducing strain. The four neighboring springs cause a net force to act on each node. We restrict the movement of the boundary layer springs, allowing motion only *along* the length of the boundary, but not normal to it.

An iterative scheme is utilized, which describes the successive decrease in natural length of each spring with time. The same rule was used earlier by Sadhukhan *et al* [12].

$$d_{\tau+1} = d_\tau(1 - b/r^\tau) \tag{1}$$

where $d_{\tau+1}$ and d_τ represent respectively the natural lengths between two nodes in the $(\tau + 1)$th and τth time steps, b is a constant and r is a parameter which controls the rate of decrease in the natural length from one time step to the next higher time step. This empirical rule causes the shrinking rate to decrease gradually with time, which is realistic. The power law anticipates the self-similarity observed in the process [13].

In [11], equation (1) is integrated and given a form more amenable to the present MD formulation. Equation (1) can be written as

$$d_\tau = \exp(br^{-\tau}/\ln r). \tag{2}$$

In the present paper we use the same form.

d_τ is normalized to d_0 at $n = 0$. b has been assigned the value 0.05 and $r = 1.1$ in this paper. When τ is large enough, the natural lengths saturate to a minimum value $d_{\min}$ and there is hardly any subsequent change. The parameters b and r are chosen such that finally $d_{\min}$ saturates to a value of about 60–70% of d_0.

The molecular dynamics proceeds as follows. As the system dries, each node is acted on by a net force determined by shrinkage of the four adjacent nearest neighbor springs. Even for the pure clay system, unbalanced forces arise due to the boundary condition imposed at the four sides. For $Pr \neq 1$ additional asymmetric forces arise due to the difference in parameters for the P–P, C–C and P–C type springs. So each node takes up a new position after time δt, determined by $\mathbf{v}\delta t$. This procedure is equivalent to a simplified form of Verlet's algorithm [11]. Here $\mathbf{v}$ is the instantaneous velocity of a particle calculated from the net force (i.e. the acceleration).

We have introduced an additional parameter n, to incorporate the comparative effect of two different timescales. One is the drying rate and the other the rate of relaxation of the system, allowing redistribution of strain in the spring network. We allow n MD steps before a spring shrinks to a new reduced length. So n steps are included in the drying time step τ.

$n = 1$ implies fastest drying, with the relaxation rate equal to the drying rate. As we shall see, the parameter n has a non-trivial role in the crack formation dynamics.

We find that the choice of $\delta t = 0.05$ gives realistic results. After every δt, the maximum force on a particle is noted. We then check whether the strain on any spring has exceeded the threshold, in which case it breaks. If a number of springs cross the threshold simultaneously, the one with the highest strain breaks. If again, there are more than one springs with the same highest strain, one is randomly chosen to break. This situation arises sometimes at the first breaking, but it rarely arises later. The next drying occurs after n such intervals.

The molecular dynamics runs until $d_{\min}$ is reached and there is no further desiccation.

4. Simulation results

We have simulated crack formation on a square network with sides 50 units long. The fraction of clay Pr has been varied from 0 to 1 in steps of 0.1. The parameters are designated as follows: $S(i, j)$ represents the spring constant of the spring connecting sites of type i and type j. Here i and j can be either P or C. The breaking threshold $B_{\text{th}}(i, j)$ is the maximum strain that the spring can withstand. If the threshold strain is exceeded, the spring breaks and the gap becomes part of a crack. The parameter n, representing the relaxation time allowed before the next drying step, has been varied from 1 to 10 in the present case. The parameters $b = 0.05$ and $r = 1.1$ have not been varied in this paper.

The values of the seven parameters affect the crack morphology very strongly. We report results for several parameter sets, for different compositions (i.e. Pr). The breaking threshold $B_{\text{th}}(\text{P}, \text{P})$ has been permanently fixed at a very large arbitrary value, so we assume that the polymer–polymer bonds never break. We present results for some specific combinations of parameters in order to identify the effect of each.

4.1. The effect of Pr variation with n = 10, and different S and B_{th}

We start with the spring parameters $S(\text{C}, \text{C}) = S(\text{P}, \text{C}) = 1.0$ and $S(\text{P}, \text{P}) = 0.1$. The thresholds are taken as $B_{\text{th}}(\text{P}, \text{C}) = 0.2$ and $B_{\text{th}}(\text{C}, \text{C}) = 0.0001$ and $n = 10$. So with this set of parameters, polymer–polymer bonds are less stiff and deform more than polymer–clay and clay–clay ones. On the other hand, the clay–clay bond breaks more easily than the clay–polymer one. The drying rate is slower than the relaxation rate. These parameters seem physically reasonable. We look at the change in the pattern as Pr varies.

The set of figures 7 shows the successive time development of cracks in the pure clay sample ($Pr = 1$). The results look very realistic when compared with the experimental crack patterns for pure laponite. The hierarchical network formed by older cracks widens as new finer cracks open up. This mimics the time development in the experiments quite well. As we decrease Pr, introduction of polymer introduces disorder in the pattern. This is shown in two sets of figures 8 and 9 with $Pr = 0.7$ and 0.5 respectively.

As long as $0.5 < Pr < 1.0$, the final pattern consists of fragmented irregular pieces, but at $Pr = 0.5$, the final pattern has a continuous network of unbroken bonds spanning the system. This is reminiscent of a percolation transition on a square lattice when bonds are broken randomly [14].

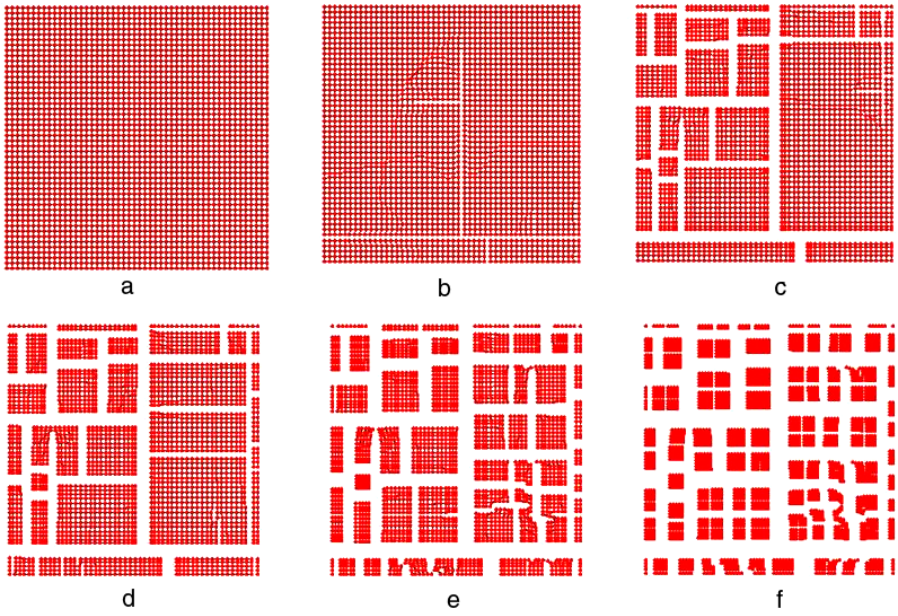

Figure 7. Patterns (a)–(f) show successive stages in the simulation of the crack network in the pure clay sample ($Pr = 1$). Details of the parameters are given in the text.

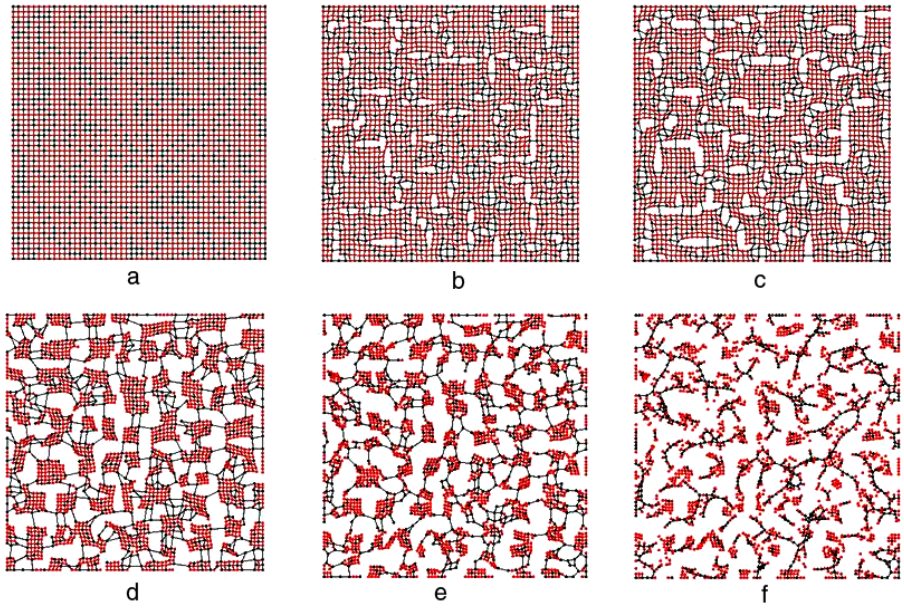

Figure 8. Patterns (a)–(f) show successive stages in the simulation of the crack network in the sample with 70% clay and 30% polymer ($Pr = 0.7$). The final pattern is still fragmented. Details of the parameters are given in the text.

4.2. The effect of varying n with the other parameters the same as in section 4.1

Now let us see the effect of changing n. Figure 10 compares patterns formed with $n = 1$ and 10 for three different values of Pr. The upper set with $n = 1$ has a larger number of broken bonds than the corresponding $n = 10$ set below, as expected. An interesting result is obtained on plotting the number of broken bonds as a function of $(1 - Pr)$ for different values of n (see figure 11). As the clay fraction increases from 0 to 1, for $n = 1$, there is a monotonic increase in the number of broken bonds in the final desiccated pattern, but for higher n, there is a peak at $Pr \sim 0.7$. The peak implies that for this combination of parameters, the effective breaking probability for P–C bonds is larger than that for C–C bonds. According to our assumption, P–P bonds never break.

4.3. Equal breaking thresholds B_{th}; only the spring constants S are different

The parameters taken here are $S(\mathrm{P,P}) = 0.2$, $S(\mathrm{C,C}) = S(\mathrm{P,C}) = 1$, $B_{\mathrm{th}}(\mathrm{P,C}) = B_{\mathrm{th}}(\mathrm{C,C}) = 0.0001$ and $n = 10$ (see figure 12). The P–P bonds always have an infinite breaking threshold. We see that even with equal breaking thresholds,

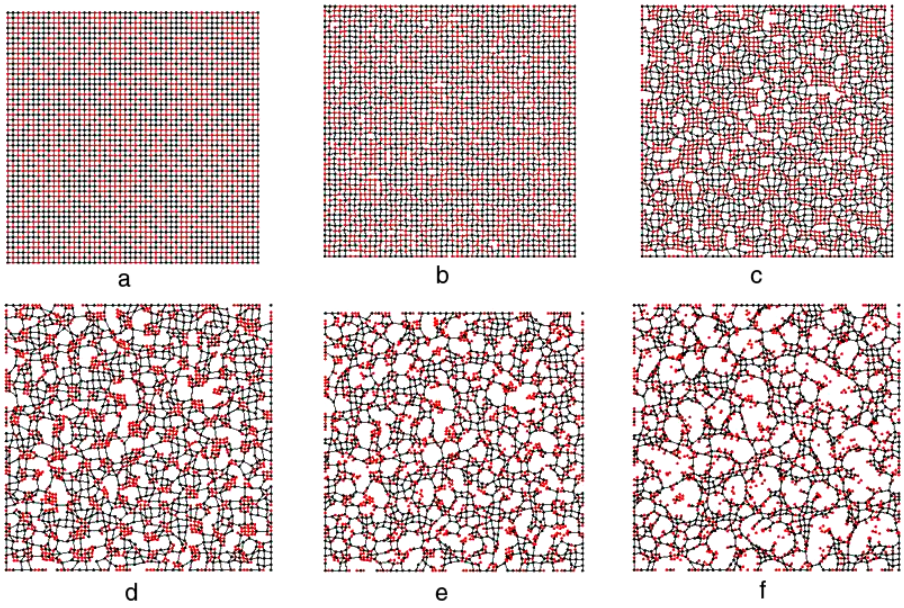

Figure 9. Patterns (a)–(f) show successive stages in the simulation of the crack network in the sample with 50% clay and 50% polymer ($Pr = 0.5$). The final pattern now has a continuous network of unbroken bonds spanning the sample.

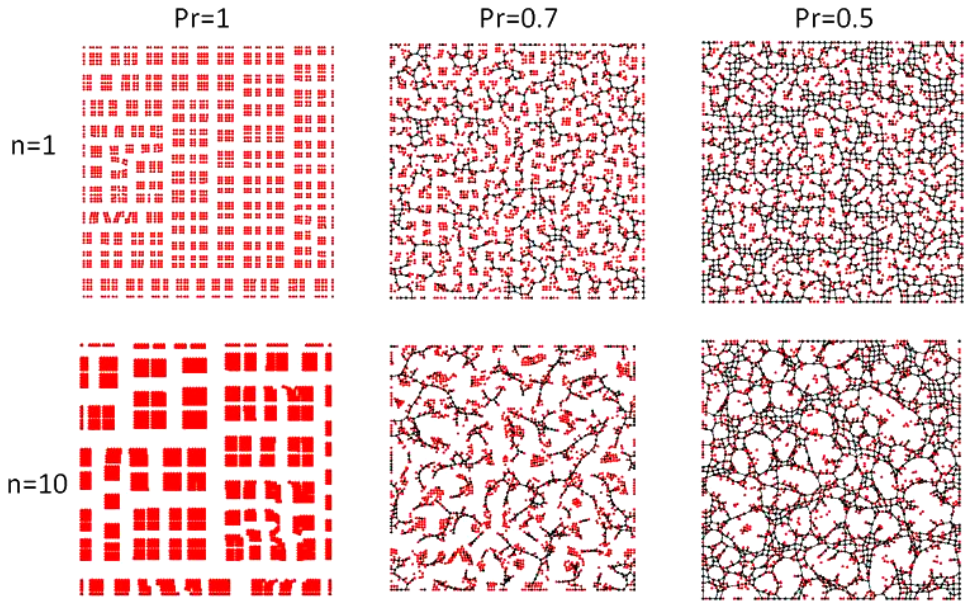

Figure 10. The upper set of figures shows the crack development with $n = 1$, and the lower that with $n = 10$, for three different compositions. Details of the parameters are given in the text.

the difference in spring parameters gives non-trivial results. Patterns for low Pr are also shown here. For $Pr = 0.1$, i.e. a predominantly polymer film with 10% clay, we have a continuous polymer film with some holes, as observed in the experiment. The holes in the simulated pattern are rather rounded compared to the experimental sample ones (see figure 1). The transition to the fragmented film occurs here between $Pr = 0.4$ and 0.5.

5. Discussion

Let us look at finer details of some of the features observed experimentally. It is rather surprising that as Pr is increased, the average ped size decreases and the area covered by the cracks *increases* (figure 4) before the transition to the continuous film. The simulation, however, shows a somewhat similar behavior, since for $n \geqslant 5$ the number of broken bonds becomes higher for $Pr = 0.7$ than for $Pr = 1.0$. For Pr lower than 0.7 the film is continuous. This shows that n larger than 1 represents a physically realistic situation, i.e. in our experiment drying is slower than relaxation.

The system size that we have taken for the simulation is not large enough for calculating the fractal dimension of the peds, but the irregular appearance of the ped outline looks realistic and similar to experimental observations. On the

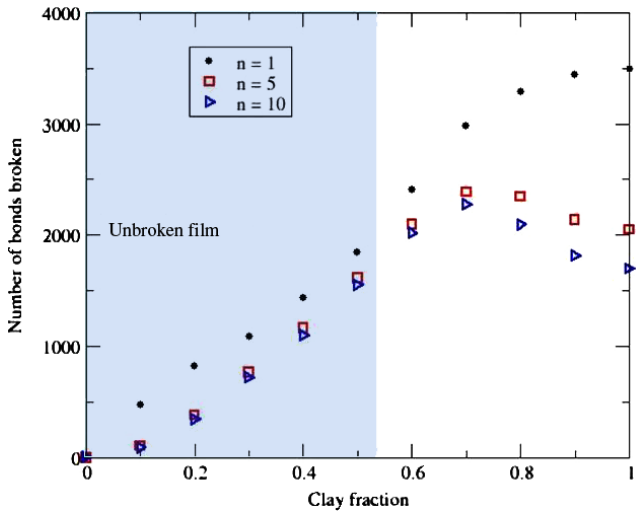

Figure 11. The number of bonds finally broken versus Pr for $n = 1$, 5 and 10 is shown. For $n = 5$ and 10, there is a peak at $Pr = 0.7$, whereas for $n = 1$ the increase is monotonic, with a tendency to saturate after $Pr = 0.7$. The regime where a continuous spanning network is present is indicated by the shaded rectangle on the left.

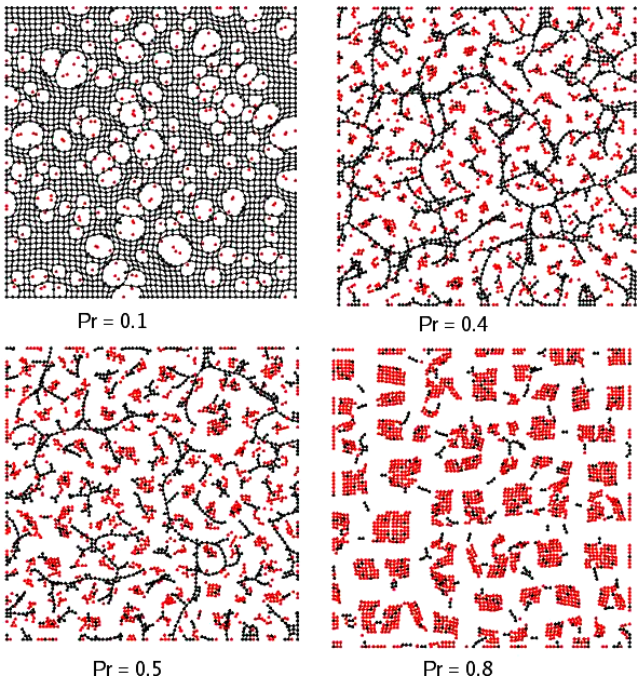

Figure 12. Crack simulation with different spring constants but the same breaking threshold. The parameters taken here are $S(\mathrm{P,P}) = 0.2$, $S(\mathrm{C,C}) = S(\mathrm{P,C}) = 1$, $B_{\mathrm{th}}(\mathrm{P,C}) = B_{\mathrm{th}}(\mathrm{C,C}) = 0.0001$ and $n = 10$. The P–P bonds always have an infinite breaking threshold.

whole, the simulation results presented are in good qualitative agreement with the experiments discussed in section 1. This shows that the physical basis of the algorithm is realistic. It will be useful to calculate actual measurable material properties, such as Young's modulus and the hardness from the spring parameters as was done by [16].

A more detailed simulation study with systematic variation of all seven parameters is in progress, but in this preliminary report we can already show the striking effect of varying the relative drying and relaxation rates, as well as the spring parameters. There are other experimental conditions which have been found to affect the crack patterns in clay significantly, such as the film thickness and the nature of the substrate.

It is well known that the average ped size scales with thickness [17] and the cumulative crack area at different resolutions can be collapsed onto a master curve on scaling by thickness [13]. It will be interesting to see whether these features are present for clay–polymer mixtures as well. For pure clay samples it was found that after excess water has evaporated from the top of the suspension, the drying rate changes from around 0.01 to 0.002 g s^{-1} [13]. The changeover indicates a transition in the nature of the cracks. Such studies are yet to be done for the polymer–clay mixtures.

The effect of the substrate is also significant. Previous work comparing cracks on polypropylene (PP) and glass substrates [12] showed that on glass cracks are much wider but less in number than those on PP. This is probably a combined effect of the hydrophobicity and roughness of the surface. Crack patterns in polymer–clay composites are likely to show a richer dependence on the substrate characteristics, particularly as the substrate–film interactions may be quite different for the two constituents.

So there are several new avenues to explore as regards polymer–clay composites which are of great interest currently [3, 4]. Polymers have become indispensable as versatile materials in numerous applications for several decades. It is found that mechanical properties of industrially applied polymers improve on addition of clay. Polymer electrolytes with clay inclusion [15] have better electrical properties. The present study adds a new set of observations to this fast developing field of clay–polymer composites.

The study of desiccation cracks is now a rich topic with many excellent experimental [18, 8, 5, 19, 20] as well as simulation [7, 16, 6, 21, 11] papers reported. Crack studies on disordered materials and composites are less reported. The work of Urabe *et al* [16] is closely related to our work. They study a disordered network with hard and soft springs on a triangular lattice. They also report a non-monotonic behavior of the number of broken springs on composition variation. This is attributed to the tortuous paths taken by the propagating crack in the disordered lattice. Spring network models with breaking and slipping of springs has been reported also by [7].

Other fascinating features related to crack formation are three-dimensional columnar joints [22] and memory effects [18]. Electric fields are also found to affect crack formation [23].

6. Conclusions

To conclude, we have presented a study of desiccation crack formation in clay–polymer composites, through experiments and simulation. Experimentally observed changes in the morphology of the crack network are reproduced quite well by a simple two-dimensional spring network model. We shall

try to correlate the model spring parameters of the constituents with measurable properties such as the elastic constants and see whether it is possible to predict properties of the composite.

Acknowledgment

Soma Nag is grateful to UGC, Government of India, for a research fellowship.

References

[1] Mal D, Sinha S, Mitra S and Tarafdar S 2004 *Physica* A **346** 110
[2] Maitra M, Middya T R, De U and Tarafdar S 2004 *Ionics* **10** 68
[3] Paul D R and Robeson L M 2008 *Polymer* **49** 3187
[4] Chen H-W and Chang F-C 2001 *Polymer* **42** 9763
[5] Shorlin K A and de Bruyn J R 2000 *Phys. Rev.* E **61** 6950–7
[6] Kitsunezaki S 1999 *Phys. Rev.* E **60** 6449
Kitsunezaki S 2009 *J. Phys. Soc. Japan* **78** 064801
[7] Komatsu T S and Sasa S 1997 *J. Appl. Phys.* **36** 391–5
[8] Bohn S, Platkiewicz J, Andreotti B, Adda-Bedia M and Couder Y 2005 *Phys. Rev.* E **71** 046215
[9] Mandelbrot B B 1977 *Form, Chance and Dimension* (San Francisco, CA: Freeman)
[10] Blaudeck P, Seeger S, Schulzsky C, Hoffmann K H, Dutta T and Tarafdar S 2006 *J. Phys. A: Math. Gen.* **39** 1609
[11] Sadhukhan S, Prehl J, Blaudeck P, Hoffmann K H, Dutta T and Tarafdar S 2008 *Eur. Phys. J.* E **27** 391
[12] Sadhukhan S, Roy Majumder S, Mal D, Dutta T and Tarafdar S 2007 *J. Phys.: Condens. Matter* **19** 356206
[13] Mal D, Sinha S, Mitra S and Tarafdar S 2006 *J. Phys. Soc. Japan* **76** 014801
[14] Stauffer D and Aharony A 1994 *Introduction to Percolation Theory* 2nd edn (London: Taylor and Francis)
[15] Pradhan D K, Choudhary R N P, Samantaray B K, Thakur A K and Katiyar R S 2009 *Ionics* **15** 345
[16] Urabe C and Takesue S 2008 arXiv:0812.4899 [cond-mat, soft]
[17] Groisman A and Kaplan E 1994 *Europhys. Lett.* **25** 415
[18] Nakahara A and Matsuo Y 2005 *J. Phys. Soc. Japan* **74** 1362
[19] Allain C and Limat L 1995 *Phys. Rev. Lett.* **74** 2981
[20] Leung K and Neda Z 2000 *Phys. Rev. Lett.* **85** 662
[21] Colina H and Roux S 2000 *Eur. Phys. J.* E **1** 189
[22] Goehring L, Lin Z and Morris S W 2006 *Phys. Rev.* E **74** 036115
[23] Mal D, Sinha S, Middya T R and Tarafdar S 2008 *Appl. Clay Sci.* **39** 106